**Technical Paper**
J. Astron. Space Sci. 35(4), 287-293 (2018)
https://doi.org/10.5140/JASS.2018.35.4.287

JASS Journal of Astronomy and Space Sciences

# Characteristics of Relative Navigation Algorithms Using Laser Measurements and Laser-GPS Combined Measurements

**Dae-Eun Kang, Sang-Young Park†, Jihae Son**
Department of Astronomy, Yonsei University, Seoul 03722, Korea

This paper presents a satellite relative navigation strategy for formation flying, which chooses an appropriate navigation algorithm according to the operating environment. Not only global positioning system (GPS) measurements, but laser measurements can also be utilized to determine the relative positions of satellites. Laser data is used solely or together with GPS measurements. Numerical simulations were conducted to compare the relative navigation algorithm using only laser data and laser data combined with GPS data. If an accurate direction of laser pointing is estimated, the relative position of satellites can be determined using only laser measurements. If not, the combined algorithm has better performance, and is irrelevant to the precision of the relative angle data between two satellites in spherical coordinates. Within 10 km relative distance between satellites, relative navigation using double difference GPS data makes more precise relative position estimation results. If the simulation results are applied to the relative navigation strategy, the proper algorithm can be chosen, and the relative position of satellites can be estimated precisely in changing mission environments.

**Keywords**: relative orbit navigation, satellite formation flying, global positioning system (GPS), laser measurement

## 1. INTRODUCTION

As satellite formation flying technology has advanced, it has become possible to perform several space missions that could not be performed with a single satellite. In the Gravity Recovery and Climate Experiment (GRACE) mission, two satellites flying in formation gathered data for the Earth gravitational model (Kroes et al. 2005). TerraSAR-X and TanDEM-X were flying in formation to generate the global digital elevation model (DEM) using synthetic aperture radar (SAR) (Krieger et al. 2007). PRISMA mission also navigated using relative positions based on global positioning system (GPS) (Candela et al. 2016). By using precise relative navigation, collision avoidance could also be maintained (Hwang et al. 2013). Precise relative navigation is required to succeed in these various formation flying missions. Various studies such as a satellite relative dynamic model (Park et al. 2009) have been conducted to provide precise relative navigation. In particular, the means to provide observations to improve relative navigation have been studied. The relative navigation algorithms are modified from the algorithms of absolute satellite navigation (Shin et al. 2016; Kim et al. 2017; Lee et al. 2017a, b). Fundamentally, relative navigation can be performed using GPS signals (Montenbruck et al. 2002). Park et al. (2008) and Sim et al. (2009) presented relative navigation algorithms based on the extended Kalman filter (EKF) and unscented Kalman filter (UKF) using GPS measurements. The relative navigation performance can be improved by using measurements other than GPS data. Recently, relative navigation algorithms using a miniaturized femtosecond laser distance meter have been developed. Jung et al. (2012) introduced a relative navigation algorithm based on laser measurements and laser pointing vectors. Lee et al. (2015) introduced a laser-based relative navigation algorithm using GPS measurements. It showed better performance than an algorithm using only GPS measurements. Furthermore, it was more precise than the algorithm using only laser measurements when the error of the angle data was large. Oh et al. (2016) improved carrier-phase differential GPS (CDGPS) by applying the laser measurements to GPS integer



**Received** 27 OCT 2018 **Revised** 12 NOV 2018 **Accepted** 15 NOV 2018
†**Corresponding Author**
Tel: +82-2-2123-5687, E-mail: spark624@yonsei.ac.kr
ORCID: https://orcid.org/0000-0002-1962-4038

ambiguity estimation. The relative navigation algorithm by Oh et al. (2016) had not been compared with the other methods. The algorithms were verified using theoretically simulated laser measurement data that did not consider the hardware properties of the instrument. Lee et al. (2018) presented relative navigation using intermittent laser-based measurement data.

In this study, the performance of the previous algorithms (Jung et al. 2012; Lee et al. 2015; Oh et al. 2016) is compared under various conditions and with improved laser measurement data that includes the hardware properties of the instrument. Numerical simulations are conducted on hardware-in-the-loop simulator (HILS) developed by Park et al. (2010). Each navigation method has different characteristics, which are reflected in the simulation results. By utilizing the results of this study, a satellite relative navigation strategy could be figured out according to the space operating environments. Based on the simulation results, we selected the algorithm with the highest performance among the three, according to the operating environment and identified the points where the performance-rank changed. Based on pre-determined points, a strategy was developed to have the best performance among the navigation algorithms loaded on the satellites, by switching to an appropriate algorithm whenever the environment changed. First, coordinate systems and the algorithms used in this research are explained briefly. Then, the simulation results are analyzed. Finally, a relative navigation strategy is presented based on the simulation results.

## 2. COORDINATE SYSTEM

In this research several coordinate systems were used. The absolute orbit of satellites was determined in Earth-centered, Earth-fixed (ECEF) coordinates using GPS data. The determined orbit was transformed to Earth-centered inertial (ECI) coordinates to be utilized for relative orbit determination. Fig. 1 shows the relative coordinate systems used to describe a relative position of a deputy satellite in relation to the chief satellite. The relative orbit of the deputy satellite is determined in RSW coordinates and spherical coordinates. The center of RSW coordinates is the center-of-mass of the chief satellite. The radial direction of the chief satellite from Earth is set to an x-axis. A normal direction of the chief satellite's orbit is set to a z-axis. A velocity direction of the chief satellite perpendicular to the x-axis and z-axis is set to a y-axis. In spherical coordinates, parameter $\rho$ means the intersatellite distance (between the chief and the deputy). Parameters $\theta$ and $\varphi$ mean angular displacement from the x-axis on the x-y plane and from the x-y plane to the z-axis, respectively.

## 3. RELATIVE NAVIGATION ALGORITHMS

In this research, the performance of three algorithms was compared. Table 1 shows the technical characteristics of the algorithms. Algorithm 1 uses only laser measurements to determine the position of the deputy satellite. Algorithm 2 and 3 use both laser measurements and differences of GPS measurements. Algorithm 1 and 2 estimate the position of the deputy satellite in spherical coordinates, which are then converted to RSW coordinates. Because of the conversion, the error of the angles has a large effect on positioning error when the distance between the satellites is far. On the other hand, Algorithm 3 directly estimates the position in RSW coordinates. The algorithms determine the relative orbit in real time using EKF. In this paper, the explanation of the EKF procedure is omitted because it is a well-known method.

### 3.1 Algorithm 1: Laser-Only Relative Navigation

The relative orbit of the deputy can be determined using laser ranging data and the direction angle of the laser (Jung et al. 2012). Eq. (1) is the state vector. Position and velocity in spherical coordinates are estimated (see Fig. 2). Below, $\rho_{CD}$ & $\dot{\rho}_{CD}$ indicate the inter-satellite range and range rate between the chief satellite and the deputy satellite.

$$\vec{x} = [\rho_{CD} \quad \theta \quad \varphi \quad \dot{\rho}_{CD} \quad \dot{\theta} \quad \dot{\varphi}]^T \tag{1}$$

Eq. (2) indicates the measurement data, which consists

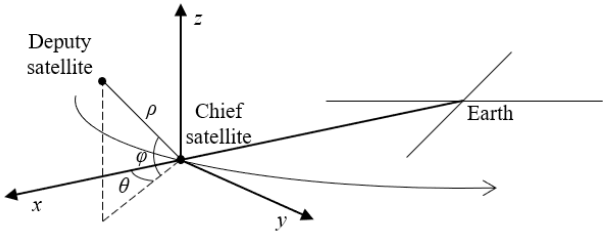


**Fig. 1.** Chief-centered relative coordinate systems: Position of the deputy satellite is represented with RSW coordinates and spherical coordinates.

**Table 1.** Technical characteristics of the algorithms

| | Algorithm 1 | Algorithm 2 | Algorithm 3 |
|---|---|---|---|
| Laser | State estimation (directly) | State estimation (directly) | GPS integer ambiguity estimation |
| GPS | Not use | Single difference | Double difference |
| Attitude information | Use | Not use | Not use |
| Filter | EKF | EKF | EKF |
| States vectors' coordinates | Spherical | Spherical | RSW |

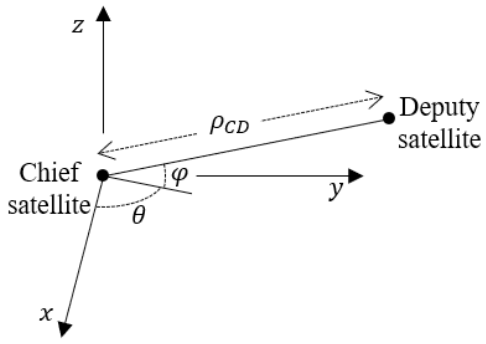


**Fig. 2.** Elements of the state vector in Algorithm 1: They are represented in spherical coordinates.

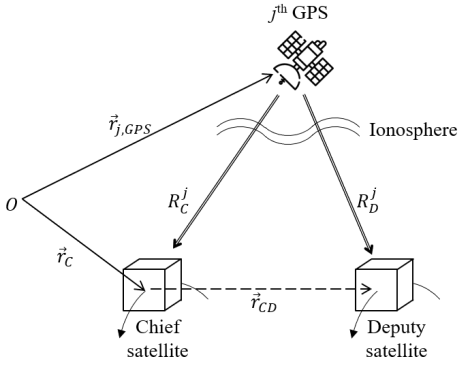


**Fig. 3.** Concept of the single difference of GPS in Algorithm 2: Pseudo-range values of the chief and the deputy satellites have the same ionospheric path delay error.

of range data $L$ measured by laser, and laser pointing angle $\hat{\theta}$, $\hat{\varphi}$. The pointing vector is estimated based on attitude information.

$$\vec{z} = [L \quad \hat{\theta} \quad \hat{\varphi}]^T \tag{2}$$

Eq. (3) is the measurement model used in EKF. The H matrix, a Jacobian matrix of the measurement data, was derived from Eq. (3).

$$\vec{y} = [\rho_{CD} + \kappa\dot{\rho}_{CD} \quad \theta \quad \varphi]^T \tag{3}$$

$$H = \frac{\partial\vec{y}}{\partial\vec{x}} = \begin{bmatrix} 1 & 0 & 0 & \kappa & 0 & 0 \\ 0 & 1 & 0 & 0 & 0 & 0 \\ 0 & 0 & 1 & 0 & 0 & 0 \end{bmatrix} \tag{4}$$

The laser measurement data $L$ shows drift due to the range rate $\dot{\rho}_{CD}$ (Jung et al. 2012). The scale factor of the drift is $\kappa$. The error levels of the measurement data were determined by laser distance meter specification and attitude-determination error. The estimation result in spherical coordinates is directly related to the measurement error. In particular, large attitude determination errors make the performance of relative navigation worse because the inter-satellite range increases.

### 3.2 Algorithm 2: Laser-GPS Combined Relative Navigation

The relative orbit of the deputy satellite with respect to the chief satellite can be determined by using laser ranging data and GPS data (Lee et al. 2015). Algorithm 1 is affected by the attitude determination precision. To compensate for this defect, Algorithm 2 utilizes the single difference of the GPS pseudo-range data instead of the attitude information. The pseudo-range includes errors caused by clock bias, ionospheric path delay, and some other terms. The ionospheric path delay and the GPS satellite's clock offset terms can be neglected by subtracting the pseudo-ranges of the chief and the deputy satellites (Montenbruck et al. 2002). Eq. (5) is the state vector estimated by Algorithm 2. The last element $\delta t_{CD}$ is the difference between the GPS clock bias in the chief and the deputy satellites.

$$\vec{x} = [\rho_{CD} \quad \theta \quad \varphi \quad \dot{\rho}_{CD} \quad \dot{\theta} \quad \dot{\varphi} \quad \delta t_{CD}]^T \tag{5}$$

Eq. (6) indicates the measurement data.

$$\vec{z} = [L \quad R_{CD}^1 \quad \cdots \quad R_{CD}^n]^T \tag{6}$$

This data consists of laser measurement data L and differences between the pseudo-range data of the chief and the deputy satellites from the $j^{th}$ GPS satellite $R_{CD}^j = R_D^j - R_C^j$, $j = 1, \cdots, n$. Eq. (7) is a measurement model.

$$\vec{y} = \begin{bmatrix} \rho_{CD} + \kappa\dot{\rho}_{CD} \\ \left|\vec{r}_C + \vec{r}_{CD} - \vec{r}_{1,GPS}\right| - \left|\vec{r}_C - \vec{r}_{1,GPS}\right| + c\delta t_{CD} \\ \vdots \\ \left|\vec{r}_C + \vec{r}_{CD} - \vec{r}_{n,GPS}\right| - \left|\vec{r}_C - \vec{r}_{n,GPS}\right| + c\delta t_{CD} \end{bmatrix} \tag{7}$$

Here, $\vec{r}_C$ means the position vector of the chief satellite, $c$ is the speed of light, and $\vec{r}_{CD}$ means the relative position vector of the deputy satellite from the chief satellite. The term $\vec{r}_{j,GPS}$, $j = 1, \cdots, n$ means the position vector of the $j^{th}$ observable GPS satellite (see Fig. 3).

Eq. (8) is the H matrix derived from Eq. (7).

$$H = \frac{\partial\vec{y}}{\partial\vec{x}} = \begin{bmatrix} \frac{\partial}{\partial\vec{x}}(\rho_{CD} + \kappa\dot{\rho}_{CD}) \\ \frac{\partial}{\partial\vec{x}}\left(\left|\vec{r}_C + \vec{r}_{CD} - \vec{r}_{1,GPS}\right| + c\delta t_{CD}\right) \\ \vdots \\ \frac{\partial}{\partial\vec{x}}\left(\left|\vec{r}_C + \vec{r}_{CD} - \vec{r}_{1,GPS}\right| + c\delta t_{CD}\right) \end{bmatrix} \tag{8}$$

The relative position of the chief to the GPS satellites is

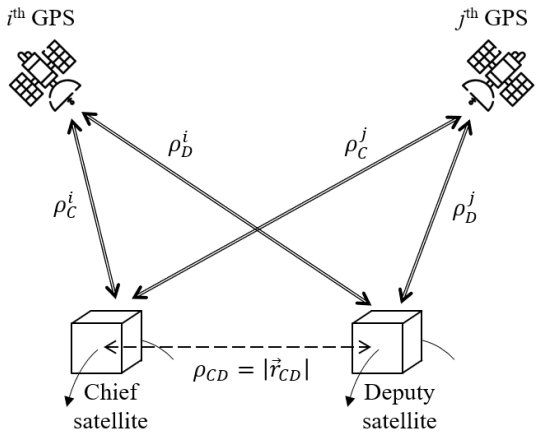


**Fig. 4.** Concept of the double difference of GPS in Algorithm 3.

omitted because it is irrelevant to the relative orbit of the deputy satellite. The pseudo-range data is smoothed using the carrier phase data.

### 3.3 Algorithm 3: Laser-CDGPS Combined Relative Navigation

The carrier-phase differential GPS (CDGPS) can be improved with laser measurement data (Oh et al. 2016). In CDGPS, the double difference of the pseudo-range and carrier-phase are used. It is essential to determine the GPS integer ambiguity accurately to utilize the carrier-phase measurements. In other words, a representative cause of error of CDGPS is failure to estimate GPS integer ambiguity. By supplementing the laser measurement data at the sub-millimeter level, the success rate of the integer ambiguity determination increased. As a result, it improved the performance of the CDGPS. The state vector includes variations of the position $\delta\vec{r}_C$ and the velocity $\delta\dot{\vec{r}}_C$ of the chief satellite, as well as the relative position $\delta\vec{r}_{CD}$ and the relative velocity $\delta\dot{\vec{r}}_{CD}$ of the deputy satellite because this algorithm uses the linearized GPS measurement model. It also includes integer ambiguity (see Eq. 9).

$$\vec{x} = \begin{bmatrix} \delta\vec{r}_C & \delta\dot{\vec{r}}_C & \delta\vec{r}_{CD} & \delta\dot{\vec{r}}_{CD} & \delta t_{CD} & N_{CD}^{ij} \end{bmatrix}^T \tag{9}$$

$$\begin{aligned} N_{CD}^{ij} &= N_{CD}^{j} - N_{CD}^{i} \\ &= N_D^j - N_C^j - N_D^i + N_C^i \end{aligned}$$

In Eq. (9), $N_C^j$ means the integer ambiguity of the carrier-phase from the $j^{th}$ GPS satellite to the chief satellite and $N_{CD}^{ij}$, element of the state vector, is the double difference of the integer ambiguities. Three kinds of measurement data were used. The double difference pseudo-range data $R_{CD}^{ij}$ were modeled as follows:

$$R_{CD}^{ij} - \rho_{CD}^{ij} = \left(\hat{e}_{CD}^{ij}\right)^T \delta\vec{r}_C + \left(\hat{e}_D^{ij}\right)^T \delta\vec{r}_{CD} + c\delta t_{CD} \tag{10}$$

where $\rho_C^j$ is the relative distance between the chief satellite and $j^{th}$ GPS satellite (see Fig. 4), $\hat{e}_D^{ij}$ is the unit vector of difference between the pseudo-range data of the deputy satellite from $i^{th}$ and $j^{th}$ GPS satellites.

Similarly, the double difference carrier phase data $\Phi_{CD}^{ij}$ was modeled as follows:

$$\lambda\Phi_{CD}^{ij} - \rho_{CD}^{ij} = \left(\hat{e}_{CD}^{ij}\right)^T \delta\vec{r}_C + \left(\hat{e}_D^{ij}\right)^T \delta\vec{r}_{CD} + \lambda N_{CD}^{ij} \tag{11}$$

where $\lambda$ denotes wavelength. The laser measurement data was modeled as follows:

$$\begin{aligned} &L - (\rho_{CD^*} + \kappa\dot{\rho}_{CD^*}) = (\hat{r}_{CD^*})^T \delta\vec{r}_{CD} \\ &+ \kappa\frac{1}{\rho_{CD^*}}\left\{\left(\dot{\vec{r}}_{CD^*}\right)^T - \dot{\rho}_{CD^*}(\hat{r}_{CD^*})^T\right\}\delta\vec{r}_{CD} + \kappa(\hat{r}_{CD^*})^T\delta\dot{\vec{r}}_{CD} \end{aligned} \tag{12}$$

The left sides of Eq. (10–12) involve the measurement data of the EKF. The right sides are the measurement model that the H matrix is derived from.

$$H = \frac{\partial\vec{y}}{\partial\vec{x}} = \begin{bmatrix} \left(\hat{e}_{CD}^{ij}\right)^T & \emptyset_{n\times 3} & \left(\hat{e}_D^{ij}\right)^T & \emptyset_{n\times 3} & c_{n\times 1} & \emptyset_{n\times(n-1)} \\ \left(\hat{e}_{CD}^{ij}\right)^T & \emptyset_{(n-1)\times 3} & \left(\hat{e}_D^{ij}\right)^T & \emptyset_{(n-1)\times 3} & \emptyset_{(n-1)\times 1} & \lambda_{(n-1)\times(n-1)} \\ \emptyset_{1\times 3} & \emptyset_{1\times 3} & (\hat{r}_{CD^*})^T + \kappa\frac{1}{\rho_{CD^*}}\left\{\left(\dot{\vec{r}}_{CD^*}\right)^T - \dot{\rho}_{CD^*}(\hat{r}_{CD^*})^T\right\} & \kappa(\hat{r}_{CD^*})^T & \emptyset_{1\times 1} & \emptyset_{1\times(n-1)} \end{bmatrix} \tag{13}$$

The laser measurement terms are represented in the last row of the H matrix, which plays an important role in the laser-based baseline measurements. It increases the resolution success rate of the integer ambiguity. In particular, the laser measurements are more effective when the inter-satellite range is too far to resolve the integer ambiguity using only the GPS measurements (Oh et al. 2016).

## 4. RELATIVE NAVIGATION SIMULATION

### 4.1 Simulation Setting

The laser measurement data was generated by a laser simulation algorithm introduced in Jung et al. (2012). The laser measurement data additionally considers the hardware properties caused by electrical circuits and RF elements in the instrument (Kang et al. 2017). The generated laser measurement data has about 100 μm level error within 10 km and worse performance as the inter-satellite range increases.

The GPS signal is generated by a Spirent GSS6560 GNSS simulator, which uses the true state data of the chief and the

**Table 2.** Initial position and velocity of the satellites in ECEF coordinates

| | | X (m) | Y (m) | Z (m) | VX (m/s) | VY (m/s) | VZ (m/s) |
|---|---|---|---|---|---|---|---|
| Chief | | -5,759,481 | -3,330,404 | 1,950,961 | 3,310.365 | -2,110.809 | 6,244.731 |
| Deputy | 500 m | -5,759,753 | -3,330,465 | 1,950,897 | 3,310.167 | -2,110.751 | 6,244.552 |
| | 1 km | -5,760,310 | -3,329,756 | 1,951,302 | 3,310.129 | -2,110.952 | 6,244.182 |
| | 10 km | -5,764,918 | -3,331,629 | 1,949,686 | 3,306.410 | -2,109.635 | 6,241.149 |
| | 50 km | -5,800,941 | -3,297.968 | 1,968,038 | 3,298.424 | -2,117.805 | 6,217.353 |
| | 100 km | -5,842,445 | -3,265,494 | 1,985,140 | 3,286.179 | -2,124.554 | 6,190.139 |
| | 200 km | -5,925,581 | -3,200,430 | 2,019,424 | 3,260.823 | -2,137.293 | 6,136.190 |

**Table 3.** 3D RMS error of the relative position according to the conditions, inter-satellite range, and attitude determination error

| Algorithm | Attitude Det. error | Inter-satellite range | | | | | |
|---|---|---|---|---|---|---|---|
| | | 500 m | 1 km | 10 km | 50 km | 100 km | 200 km |
| 1 | 1″ | 0.73 | 1.83 | 9.23 | 73.33 | 141.26 | 295.75 |
| | 0.001° | 1.48 | 3.74 | 21.27 | 163.84 | 287.21 | 766.12 |
| | 0.005° | 8.19 | 10.86 | 94.51 | 486.55 | 983.41 | 3,854.15 |
| | 0.01° | 11.09 | 20.80 | 181.67 | 921.49 | 1,778.82 | 5,494.71 |
| 2 | | 16.08 | 22.78 | 58.97 | 141.07 | 284.12 | 451.48 |
| 3 | | 2.32 | 14.75 | 25.63 | 253.85 | 408.59 | 773.21 |

(Unit: mm)

deputy satellite to produce the GPS L1 signal observed by the receiver (AsteRX1 PRO) manufactured by Septentrio Inc. The GNSS simulator and the receiver are components of the HILS. They make a GPS signal reflecting the hardware properties in real time (Park et al. 2010). The true state data of the chief and the deputy satellites are simulated by numerical integration of the dynamic model, which includes acceleration due to gravitational forces (Earth, Moon, and Sun), atmospheric forces, and solar radiation pressure. In contrast, the dynamic model in the EKF only considers the J2 term as perturbation to reduce the computational burden.

To analyze the performance of each algorithm, we compared the accuracy of the simulation results of the relative distance between the satellites and the attitude determination accuracy. For the initial conditions of the chief and deputy satellites, the relative distance was set from 500 m to 200 km on a projected circular orbit (PCO). The attitude determination accuracy was set to 1″, 0.001°, 0.005°, and 0.01°. The components of the position and velocity in the ECEF frame for each of the chief and the deputy satellites are presented in Table 2. The simulations ran for 5,000 seconds and the sampling time of the GPS and laser measurement data was one second.

### 4.2 Simulation Results and Analysis

Table 3 shows the simulation results, which represent the 3D root-mean-square (3D RMS) of the relative position determination error in millimeters. The performance of Algorithm 1 deteriorates in proportion to the attitude determination error. The performances of Algorithm 2 and 3 are unrelated to the satellite attitude. As the relative distance increases, the precision decay rate of Algorithm 3 is faster than that of Algorithm 2. Algorithm 1 has a rate similar to that of Algorithm 3. When the inter-satellite range is less than 10 km, Algorithm 3 has better performance than Algorithm 2. In contrast, Algorithm 2 is more precise than Algorithm 3 when the relative distance is greater than 10 km. Figs. 5–8 show the comparison results of Algorithm 1 with the other algorithms. Algorithm 1 had the best performance when the attitude determination error was 1″ (see Fig. 5). When the deputy was closer than 10 km, the relative navigation error of Algorithm 1 was smaller than the error of the others with 0.001° attitude determination error (see Fig. 6). Figs. 7 and 8 show that Algorithm 1 is similar or worse. Consequently, the relative navigation was conducted using Algorithm 1 when the attitude determination was precise. In the other cases, an appropriate algorithm should be selected (see Table 4).

## 5. CONCLUSIONS

In this research, real-time relative navigation algorithms using the laser and GPS measurement data were assessed. Software simulation was conducted to compare the performance of the algorithms using various inter-satellite range and precision of attitude determination. For numerical evaluation, the simulation results were represented as 3D RMS error. If the high-precision attitude determination system is guaranteed, the algorithm that uses only the laser measurements can have the best navigation result. Performance degradation, however, stands out as the attitude determination precision worsens. The same performance were maintained regardless of the attitude determination error, when the laser and GPS measurements

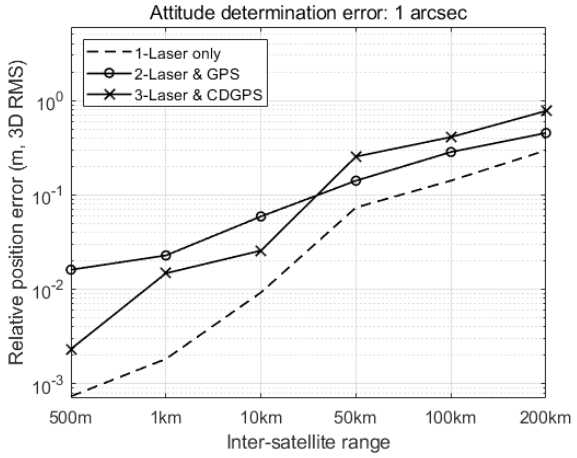


**Fig. 5.** 3D RMS error of the relative position according to inter-satellite range using Algorithm 1–3 when the attitude determination error is 1″.

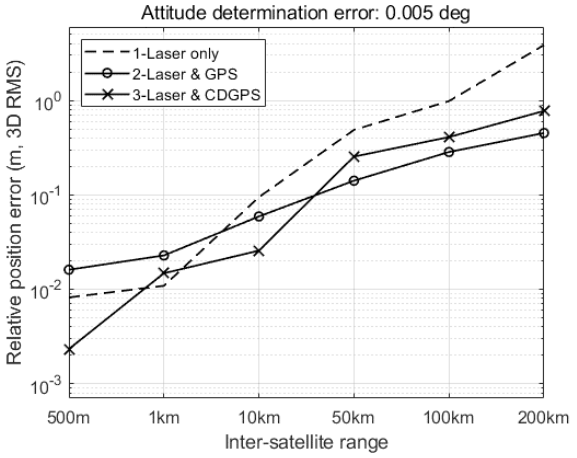


**Fig. 7.** 3D RMS error of the relative position according to inter-satellite range using Algorithm 1–3 when the attitude determination error is 0.005°.

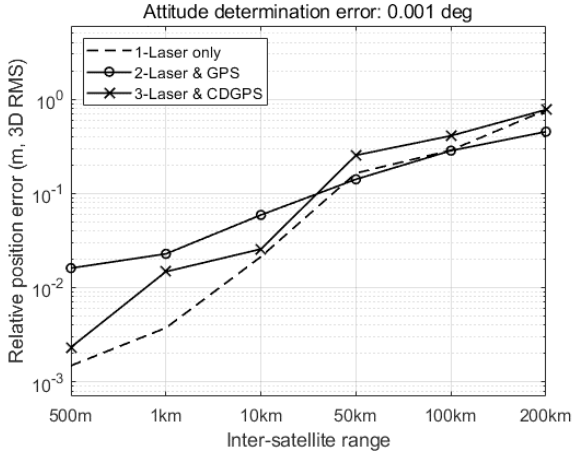


**Fig. 6.** 3D RMS error of the relative position according to inter-satellite range using Algorithm 1–3 when the attitude determination error is 0.001°.

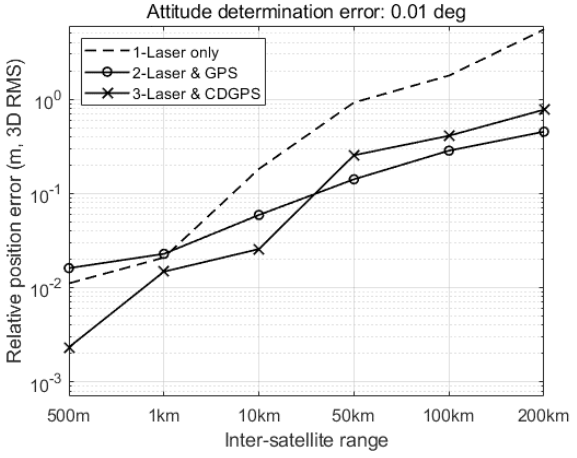


**Fig. 8.** 3D RMS error of the relative position according to inter-satellite range using Algorithm 1–3 when the attitude determination error is 0.01°.

**Table 4.** Characteristics of the relative navigation algorithms based on the simulation results

| | Algorithm 1 | Algorithm 2 | Algorithm 3 |
|---|---|---|---|
| Laser | State estimation (directly) | State estimation (directly) | GPS integer ambiguity estimation |
| GPS | Not use | Single difference | Double difference |
| Attitude information | Use | Not use | Not use |
| Filter | EKF | EKF | EKF |
| States vectors' coordinates | Spherical | Spherical | RSW |
| Dependence on attitude determination precision | High | Low | Low |
| Decay rate of precision according to the relative distance | High | Low | High |
| Proper performance condition | Attitude det. Error < 0.001° | Attitude det. Error > 0.001° | |
| | | Relative distance > 10 km | Relative distance < 10 km |

were combined. Therefore, if the deterioration of attitude determination occurs, perhaps due to such as malfunction of the attitude sensors, it would be more strategic to choose combined laser-GPS or combined laser-CDGPS relative navigation. Within about 10 km inter-satellite range, the laser-CDGPS combined relative navigation should be conducted because its error is smaller than the other's. Although the switching point of the algorithms using combined measurements is determined at around 10 km inter-satellite range, the practical point should be determined in detail by considering several conditions,

such as the characteristics of the satellite system or the mission environment. In conclusion, a reasonable relative navigation algorithm can be chosen for suitable performance based on the simulation results.

## ACKNOWLEDGMENTS

This work was supported by a Global Surveillance Research Center (GSRC) program funded by the Defense Acquisition Program Administration (DAPA) and Agency for Defense Development (ADD) of Korea.

## REFERENCES

Candela L, Formaro R, Guarini R, Loizzo R, Longo F, et al., The PRISMA mission, in 2016 IEEE IGARSS, Beijing, China, 10-15 Jul 2016.

Hwang IY, Park SY, Park C, Collision avoidance algorithm for satellite formation reconfiguration under the linearized central gravitational fields, J. Astron. Space Sci. 30, 11-15 (2013). https://doi.org/10.5140/JASS.2013.30.1.011

Jung S, Park SY, Park HE, Park C, Kim SW, et al., Real-time determination of relative position between satellites using laser ranging, J. Astron. Space Sci. 29, 351-362 (2012). https://doi.org/10.5140/JASS.2012.29.4.351

Kang DE, Park SY, Lee J, A satellite relative navigation based on hardware characteristics of femtosecond laser, Proceedings of the 3rd World Congress on Mechanical, Chemical, and Material Engineering (MCM'17), Rome, Italy, 8-10 Jun 2017.

Kim Y, Park SY, Lee E, Kim M, A deep space orbit determination software: overview and event prediction capability, J. Astron. Space Sci. 34, 139-151 (2017). https://doi.org/10.5140/JASS.2017.34.2.139

Krieger G, Moreira A, Fiedler H, Hajnsek I, Werner M, et al., TanDEM-X: a satellite formation for high-resolution SAR interferometry, IEEE Trans. Geosci. Remote Sens. 45, 3317-3341 (2007). https://doi.org/10.1109/TGRS.2007.900693

Kroes R, Montenbruck O, Bertiger W, Visser P, Precise GRACE baseline determination using GPS, GPS Solut. 9, 21-31 (2005). https://doi.org/10.1007/s10291-004-0123-5

Lee E, Park SY, Shin B, Cho S, Choi EJ, et al., Orbit determination of KOMPSAT-1 and Cryosat-2 satellites using optical wide-field patrol network (OWL-Net) data with batch least squares filter, J. Astron. Space Sci. 34, 19-30 (2017a). https://doi.org/10.5140/JASS.2017.34.1.19

Lee E, Kim Y, Kim M, Park SY, Development, demonstration and validation of the deep space orbit determination software using lunar prospector tracking data, J. Astron. Space Sci. 34, 213-223 (2017b). https://doi.org/10.5140/JASS.2017.34.3.213

Lee J, Park SY, Kang DE, Relative navigation with intermittent laser-based measurement for spacecraft formation flying, J. Astron. Space Sci. 35, 163-173 (2018). https://doi.org/10.5140/JASS.2018.35.3.163

Lee K, Oh H, Park HE, Park SY, Park C, Laser-based relative navigation using GPS measurements for spacecraft formation flying, J. Astron. Space Sci. 32, 387-393 (2015). https://doi.org/10.5140/JASS.2015.32.4.387

Montenbruck O, Ebinuma T, Lightsey EG, Leung S, A real-time kinematic GPS sensor for spacecraft relative navigation, Aerosp. Sci. Technol. 6, 435-449 (2002). https://doi.org/10.1016/S1270-9638(02)01185-9

Oh H, Park HE, Lee K, Park SY, Park C, Improved GPS-based satellites relative navigation using femtosecond laser relative distance measurements, J. Astron. Space Sci. 33, 45-54 (2016). https://doi.org/10.5140/JASS.2016.33.1.45

Park HE, Park SY, Lee SJ, Choi KH, Analysis of linear and nonlinear relative orbit dynamics for satellite formation flying, J. Astron. Space Sci. 26, 317-328 (2009). https://doi.org/10.5140/JASS.2009.26.3.317

Park IK, Park SY, Choi KH, Choi SK, Park JU, Filtering performance analyzing for relative navigation using single difference carrier-phase GPS, J. Astron. Space Sci. 25, 283-290 (2008). https://doi.org/10.5140/JASS.2008.25.3.283

Park JI, Park HE, Park SY, Choi KH, Hardware-in-the-loop simulations of GPS-based navigation and control for satellite formation flying, Adv. Space Res. 46, 1451-1465 (2010). http://doi.org/10.1016/j.asr.2010.08.012

Shin K, Oh H, Park SY, Park C, Real-time orbit determination for future Korean regional navigation satellite system, J. Astron. Space Sci. 33, 37-44 (2016). https://doi.org/10.5140/JASS.2016.33.1.37

Sim SH, Park SY, Choi KH, Autonomous real-time relative navigation for formation flying satellites, J. Astron. Space Sci. 26, 59-74 (2009). https://doi.org/10.5140/JASS.2009.26.1.059